Uncertainty quantification in a chemical system using error estimate-based mesh adaption

L. Mathelin[a], O. Le Maître[a,b]

[a] *LIMSI-CNRS, 91403 Orsay cedex, France*
[b] *CEA/Saclay/DEN/DM2S, 91191 Gif-sur-Yvette cedex, France*

Abstract

This paper describes a rigorous *a posteriori* error analysis for the stochastic solution of non-linear uncertain chemical models. The dual-based *a posteriori* stochastic error analysis extends the methodology developed in the deterministic finite elements context to stochastic discretization frameworks. It requires the resolution of two additional (dual) problems to yield the local error estimate. The stochastic error estimate can then be used to adapt the stochastic discretization. Different anisotropic refinement strategies are proposed, leading to a cost-efficient tool suitable for multi-dimensional problems. The adaptive strategies allow both for refinement and coarsening of the stochastic discretization, as needed to satisfy a prescribed error tolerance. The adaptive strategies were successfully tested on a model for the hydrogen oxidation in supercritical conditions having up to 8 random parameters. The proposed methodologies are however general enough to be also applicable for a wide class of models such as uncertain fluid flows.

Key words: uncertainty quantification, error analysis, stochastic finite elements method, adaptive mesh refinement, Polynomial Chaos

1. Introduction

With the quickly increasing computational power of modern calculators and the constant progresses of numerical methods and algorithms, it becomes affordable to deal with large problems and to simulate more and more complex physical phenomena. In a similar aim to simulate ever more realistic systems, it is also desirable to account for the uncertainty which may lie on some parameters of its mathematical model. Indeed, even so the computation may be very accurate, simulation may be of little help if the operating conditions of the physical system are not perfectly known, at the very least, to a comparable level of accuracy as the solution is sought for. In fact, as simulation tools progress, it becomes more and more crucial to propagate and quantify uncertainty on model data to assess its impact on the model solution. This is best achieved in a probabilistic framework, where the solution uncertainty is characterized by its probability law or abstract statistical quantities (*e.g.* its mean, variance, first moments, quantiles, confidence intervals, ...), for prescribed probabilistic distribution of the uncertain model data.

As far as chemical systems are concerned, uncertainty quantification is primarily needed due to the use of reduced reaction mechanisms which involves model constants (*e.g.* reaction rates) identified from experiments -or more detailed models- with a significant level of uncertainty. The main difficulty with uncertainty propagation and quantification in chemical systems is the non-linear character of the governing equations. The non-linearities in the model equations have generally for direct consequence a complex dependence (non monotonic, bifurcation, ...) of the solution with the model data with an amplification of the variability as a result [17]. This prevents using simple deterministic propagation techniques, such as local sensitivity analysis.

[☆] This work is supported by the ANR, Project ASRMEI, grant number JC08-375619
Email addresses: mathelin@limsi.fr (L. Mathelin), olm@limsi.fr (O. Le Maître)

To characterize the solution uncertainty, given a probabilistic description of the input data, the most common method is certainly the Monte-Carlo simulation approach. It basically consists in multiple resolutions of the model for a sample set of independent realizations of the uncertain data, followed by a sample set-based (or empirical) statistical characterization of the solution variability. Though robust and straightforward to implement in the context of complex or legacy codes, which here are used as black-boxes possibly running in parallel, the convergence of the empirical estimates are slow, in a Monte-Carlo simulation, such that well converged estimates require a prohibitively large number of realizations for models whose resolution is time consuming. This limitation can be partially tempered using advanced sampling strategies (Latin Hypercube Sampling, Quasi-Monte-Carlo sampling,...), but the convergence rates remain generally too low to achieve accuracy levels comparable to those of the deterministic model solvers.

The stochastic spectral method is an alternative approach to the simulation methods, where the uncertain data are thought as generating new dimensions in the model solution. One can then seek for a convergent approximation of the uncertain solution on a space spanned by suitable stochastic functionals. In practice, a parameterization of the uncertain model data is first performed using a set of independent random variables with prescribed probability distributions, followed by a projection of the solution on the space of second order functionals in the random variables. The work of Wiener [22], suggested to use standard Gaussian variables and orthogonal polynomial functionals to span the projection space, leading to the so-called Polynomial Chaos expansion (PC) of a second order random variable. The original PC expansions were used for uncertainty quantification and propagation in the seminal work of Ghanem and Spanos [7]. Later, these polynomial expansions were generalized to independent random variables with arbitrary probability measures in [23] and to dependent random variables in [20]. Initially applied in structural mechanics, [7], the PC approach has now widely spread in many application domains such as heat transfer [8, 10], flow in porous media [6], and fluid mechanics [14, 13]. The efficiency of the stochastic spectral methods comes from the fast convergence of the PC expansions, such that the variability of the solution can be accurately represented on a low dimensional stochastic space, with efficient computational procedures as a result.

Although found effective for many applications, and much faster and accurate than simulation methods (provided that the number of random variables in the parameterization is not too large), stochastic spectral methods are challenged by chemical systems whose solutions may lack regularity and exhibit steep dependences with regards to the random variables: stochastic bases of spectral polynomials are inappropriate. Instead, for these non-linear models, piecewise polynomial expansions are needed, such as the Multi-Element Generalized Polynomial Chaos (ME-GPC) [5, 21] or stochastic Multi-Wavelet (MW) bases [11, 12]. The main advantage of these representations is that they allow for discontinuous dependences and offer flexibility in the local control of the stochastic discretization by relying on polynomial functionals which have compact supports in the random variables domain. A key aspect here is the need for efficient and reliable procedures to control the stochastic discretization while keeping the overall number of terms in the expansion to a reasonable level. In this direction, an adaptation procedure was proposed in a multi-resolution framework and MW discretizations in [12, 17]. However, this adaptation algorithm used in these works relies mainly on heuristic considerations to decide further enrichment of the stochastic discretization. Instead, it would be desirable to derive rigorous estimations of the local stochastic error to trigger the stochastic discretization adaptation.

The derivation of rigorous error estimates and related adaptation strategies constitutes the main objective of the present paper which is organized as follows. In Section 2, the model equations of the uncertain chemical system are presented. This apparently simple system is selected as it is known from previous works to be actually extremely challenging [12]. Then, the stochastic discretization of the solution is introduced and the Galerkin projection of the model equations is detailed (for a given stochastic discretization). In Section 3, we present a dual-based stochastic error estimation methodology. The methodology is similar to the a posteriori error estimation technique used in the deterministic finite element context (see for instance [2]), which was extended to the stochastic framework in [15]. It requires the resolution of two adjoint problems, whose derivation is detailed. In Section 4, we discuss different adaptation strategies on the basis of the previously derived error estimate. The discussion emphasizes the issue of directional enrichment in order to limit the dimension of the resulting discretization space. In addition to the enrichment, a coarsening procedure is considered to remove some elements of the stochastic basis when they become unnecessary as time evolves.

j	reaction			$\widehat{\Gamma}_{f,j}$	γ_j	λ_j
1	$OH + H$	$\rightleftarrows$	H_2O	$1.479\ 10^{14}$	$+\infty$	3.16
2	$H_2 + OH$	$\rightleftarrows$	$H_2O + H$	$6.295\ 10^{11}$	$4.380\ 10^{-4}$	1.26
3	$H + O_2$	$\rightleftarrows$	HO_2	$8.314\ 10^{13}$	$9.879\ 10^{-14}$	1.58
4	$HO_2 + HO_2$	$\rightleftarrows$	$H_2O_2 + O_2$	$7.281\ 10^{11}$	$1.045\ 10^{-9}$	1.41
5	$H_2O_2 + OH$	$\rightleftarrows$	$H_2O + HO_2$	$3.469\ 10^{12}$	$3.382\ 10^{-9}$	1.58
6	$H_2O_2 + H$	$\rightleftarrows$	$HO_2 + H_2$	$1.696\ 10^{11}$	$7.723\ 10^{-6}$	2.00
7	H_2O_2	$\rightleftarrows$	$OH + OH$	$3.993\ 10^{1}$	$1.589\ 10^{11}$	3.16
8	$OH + HO_2$	$\rightleftarrows$	$H_2O + O_2$	$3.917\ 10^{13}$	$3.534\ 10^{-18}$	3.16

Table 1: Description of the different chemical reactions and their kinetics properties involved in the simplified mechanism.

Finally, in Section 5, the proposed algorithms are tested on problem with 2 and 8 uncertain parameters to demonstrate their effectiveness, and major findings are summarized in Section 6.

2. Uncertain chemical system

The simulation of the time-evolution of the hydrogen oxidation in supercritical conditions with uncertain settings is here considered. The problem is both complex and stiff since it involves several chemical reactions which time scales are driven by the different reactions rates varying by several or even tens of orders of magnitude from each other. However, we here focus on a simplified mechanism as already considered in [12] involving only 8 reactions and 7 chemical species. The reaction rates are obtained from experiments but their measure is difficult and their values are subjected to a large discrepancy. To account for the information provided by the discrepancy, the reaction rates are modeled as random variables and we rely on the hypothesis that they are statistically independent. This allows to re-express the whole problem in a stochastic framework. Through the equations of the chemical system problem, the uncertainty in the reaction rates leads to uncertain species content which are then random processes. Finally, the resulting problem at hand is then a 8-D time-dependent uncertainty quantification problem.

2.1. Problem settings

The chemical model describes the concentration of $n_S = 7$ species, [OH], [H], [HO_2], [O_2], [H_2O], [H_2] and [H_2O_2], through a reduced mechanism of $n_R = 8$ reactions.

The reaction rates being random, they are defined on an abstract probability space $(\Theta, \mathcal{B}, d\mu)$, Θ being the set of outcomes, $\mathcal{B}$ the associated σ-algebra and μ the probability measure. The reactions are defined by their forward and reverse rates denoted respectively $\Gamma_{f,j}(\theta)$ and $\Gamma_{r,j}(\theta)$, $j = 1, \dots, n_R$. The rates are assumed to be independent random variables with log-normal distributions characterized by their respective coefficients of variation λ_j, defined with regard to the forward rates. The coefficient of variation is related to the 95% confidence interval through:

$$\text{Prob}(\Gamma_{f,j} \in [\widehat{\Gamma}_{f,j}/\lambda_j; \widehat{\Gamma}_{f,j}\ \lambda_j]) = 0.95 \qquad \forall\, j = 1, \dots, n_R, \tag{1}$$

where $\widehat{\Gamma}_{f,j}$ is the median value of the forward rate of the j-th reaction. For each reaction, the ratio of forward and reverse rates is assumed deterministic (certain) and is denoted $\gamma_j \equiv \widehat{\Gamma}_{f,j}(\theta)/\widehat{\Gamma}_{r,j}(\theta)$ (with probability one). The reactions, median rates, coefficients of variations and forward to reverse ratii are summarized in Table 1.

2.2. Stochastic discretization

For the stochastic discretization of the model, it is convenient to parameterize the reaction rates using a set of n_R independent identically distributed (iid) random variables, $\boldsymbol{\xi}(\theta) = (\xi_1(\theta) \dots \xi_{n_R}(\theta))$, with

probability density function $p_{\boldsymbol{\xi}}(\boldsymbol{\xi})$. Since the random variables are iid, $p_{\boldsymbol{\xi}}$ has a product form:

$$p_{\boldsymbol{\xi}}(\boldsymbol{\xi}) = \prod_{j=1}^{n_R} p(\xi_j). \tag{2}$$

Without loss of generality, we shall restrict ourselves to random variables having a uniform probability onto $[-1;1]$ so that

$$p(\xi_j) = \begin{cases} 1/2, & \text{if } \xi_j \in [-1,1] \\ 0, & \text{otherwise} \end{cases} \tag{3}$$

and we define $\Omega_{\boldsymbol{\xi}} \equiv [-1;1]^{n_R}$. The random variables define an image probability space, $(\Omega_{\boldsymbol{\xi}}, \mathcal{B}_{\boldsymbol{\xi}}, p_{\boldsymbol{\xi}})$, and we denote $\mathcal{V}_{\boldsymbol{\xi}}(\Omega_{\boldsymbol{\xi}}, p_{\boldsymbol{\xi}})$ the space of second order random variables defined on the image probability space:

$$f(\boldsymbol{\xi}(\theta)) \in \mathcal{V}_{\boldsymbol{\xi}} \Rightarrow E\left[f\right] \equiv \int_{\Theta} f(\boldsymbol{\xi}(\theta) d\mu(\theta) = \int_{\Omega_{\boldsymbol{\xi}}} f(\boldsymbol{\xi}) p_{\boldsymbol{\xi}}(\boldsymbol{\xi}) d\boldsymbol{\xi} = \langle f \rangle_{\Omega_{\boldsymbol{\xi}}} < +\infty. \tag{4}$$

The set of orthogonal random polynomials Ψ for the uniform density $p_{\boldsymbol{\xi}}$ are the n_R-D Legendre polynomials [1], which satisfy

$$\int_{\Omega_{\boldsymbol{\xi}}} \Psi_i(\boldsymbol{\xi})\, \Psi_j(\boldsymbol{\xi})\, p_{\boldsymbol{\xi}}(\boldsymbol{\xi})\, d\boldsymbol{\xi} = \langle \Psi_i(\boldsymbol{\xi})\, \Psi_j(\boldsymbol{\xi}) \rangle_{\Omega_{\boldsymbol{\xi}}} = \delta_{ij} \left\langle \Psi_i^2 \right\rangle_{\Omega_{\boldsymbol{\xi}}} \qquad \forall i,j = 0,1,2,\ldots, \tag{5}$$

These polynomials form an orthogonal basis of $\mathcal{V}_{\boldsymbol{\xi}}$:

$$\mathcal{V}_{\boldsymbol{\xi}} = \text{span } \left\{\Psi_k\right\}. \tag{6}$$

For practical implementation purposes, a finite dimensional stochastic space is to be used. This is constructed by considering a finite number $(P_{\boldsymbol{\xi}} + 1)$ of polynomials to form the approximation basis. We denote

$$\mathcal{V}_{\boldsymbol{\xi}}^h = \text{span}\{\Psi_0, \ldots, \Psi_{P_{\boldsymbol{\xi}}}\} \subset \mathcal{V}_{\boldsymbol{\xi}}, \tag{7}$$

the discrete stochastic approximation space. Classically, the discrete basis consists of the polynomials with (total) degree less or equal to q such that

$$P_{\boldsymbol{\xi}} + 1 = \frac{(q + n_R)!}{q!\, n_R!}. \tag{8}$$

Using the random variable ξ_j to parameterize the rate $\widehat{\Gamma}_{f,j}$ (and $\widehat{\Gamma}_{r,j}$), the approximation of the random rates are obtained by means of an orthogonal projection on $\mathcal{V}_{\boldsymbol{\xi}}^h$; we end with

$$\Gamma_{f,j} \approx \sum_{k=0}^{P_{\boldsymbol{\xi}}} \left(\Gamma_{f,j}\right)_k\, \Psi_k(\boldsymbol{\xi}) \qquad \forall j = 1, \ldots, n_R,$$

where the projection coefficients $\left(\Gamma_{f,j}\right)_k$ have for expression:

$$\left(\Gamma_{f,j}\right)_k \left\langle \Psi_k^2 \right\rangle_{\Omega_{\boldsymbol{\xi}}} = \int_{\Omega_{\boldsymbol{\xi}}} \widehat{\Gamma}_{f,j}\, \exp^{\frac{\log \lambda_j}{1.96}\, \mathcal{T}(\xi_j)}\, \Psi_k(\boldsymbol{\xi})\, p_{\boldsymbol{\xi}}(\boldsymbol{\xi})\, d\boldsymbol{\xi}, \tag{9}$$

where $\mathcal{T}(\xi_j)$ is an isoprobabilistic mapping between $(-1,1)$ to $(-\infty,+\infty)$, such that $\mathcal{T}$ has a standard normal distribution (zero mean and unit variance). Similar expressions hold for the reverse rates.

2.3. Solution method: stochastic Galerkin projection

The model solution is fully described by the time-evolution of the state vector containing the different chemical species concentrations: $\boldsymbol{U} = ([\mathrm{OH}]\ [\mathrm{H}]\ [\mathrm{HO_2}]\ [\mathrm{O_2}]\ [\mathrm{H_2O}]\ [\mathrm{H_2O_2}])^T$. Since the model involves some random parameters, its solution is a random process defined on the image space. Therefore, we have $\boldsymbol{U} = \boldsymbol{U}(t, \boldsymbol{\xi})$. The chemical system is governed by a set of non-linear coupled stochastic ODEs. For instance the ODE for [OH] is:

$$\begin{aligned}\frac{d[\mathrm{OH}](t,\boldsymbol{\xi})}{dt} &= \Gamma_{r,1}(\boldsymbol{\xi})[\mathrm{H_2O}](t,\boldsymbol{\xi}) + \Gamma_{r,2}(\boldsymbol{\xi})[\mathrm{H_2O}](t,\boldsymbol{\xi}))[\mathrm{H}] + \Gamma_{r,5}(\boldsymbol{\xi})[\mathrm{H_2O}](t,\boldsymbol{\xi})[\mathrm{HO_2}](t,\boldsymbol{\xi}) \\ &\quad + \Gamma_{r,8}(\boldsymbol{\xi})[\mathrm{H_2O}](t,\boldsymbol{\xi})[\mathrm{O_2}](t,\boldsymbol{\xi}) - 2\Gamma_{f,7}(\boldsymbol{\xi})[\mathrm{H_2O_2}](t,\boldsymbol{\xi}). \end{aligned} \tag{10}$$

The solution is sought for $\Omega_t = [0, T]$, so initial conditions at $t = 0$ are needed; these will be considered deterministic:

$$\begin{array}{llll} [\mathrm{OH}] = 0, & [\mathrm{H_2O}] = 4.281\ 10^{-3}, & [\mathrm{H}] = 0, & [\mathrm{H_2}] = 2.060\ 10^{-6}, \\ [\mathrm{HO_2}] = 0, & [\mathrm{O_2}] = 1.040\ 10^{-6}, & [\mathrm{H_2O_2}] = 0. & \end{array} \tag{11}$$

To simplify the notations, we hereafter refer to U as any of the component of $\boldsymbol{U}$.

We further denote $\mathcal{V} \equiv L_2(\Omega_{\boldsymbol{\xi}}, \Omega_t, p_{\boldsymbol{\xi}})$ the space of second order random processes and we assume $U \in \mathcal{V}$:

$$\left|\langle U(t,\boldsymbol{\xi})U(t',\boldsymbol{\xi})\rangle_{\Omega_{\boldsymbol{\xi}}}\right| < +\infty,\ \forall t, t' \in \Omega_t, \quad \int_{\Omega_t} \left\langle U(t,\boldsymbol{\xi})^2\right\rangle_{\Omega_{\boldsymbol{\xi}}} dt < +\infty. \tag{12}$$

The set of stochastic ODEs can be formally re-expressed as

$$a(\boldsymbol{U}(t,\boldsymbol{\xi}),\boldsymbol{\xi}) = 0, \qquad p_{\boldsymbol{\xi}} - a.s., \qquad \forall\, t \in \Omega_t. \tag{13}$$

It is assumed that the problem is well posed in the sense that it has $p_{\boldsymbol{\xi}}$–almost surely a unique solution. The weak form of Eq. (13) is: find $\boldsymbol{U} \in (\mathcal{V})^{n_S}$ such that

$$A(\boldsymbol{U};\boldsymbol{\phi}) = 0, \qquad \forall \boldsymbol{\phi} = (\phi_1 \dots \phi_{n_S})^T \in (\mathcal{V})^{n_S}. \tag{14}$$

In the previous equation, the operator A is a differentiable semi-linear form defined as:

$$A(\boldsymbol{U};\boldsymbol{\phi}) \equiv \int_{\Omega_{\boldsymbol{\xi}}}\int_{\Omega_t} a(\boldsymbol{U}(t,\xi),\boldsymbol{\xi})\ \boldsymbol{\phi}(t,\boldsymbol{\xi})\ p_{\boldsymbol{\xi}}(\boldsymbol{\xi})\ dt\ d\boldsymbol{\xi} = \left\langle \int_{\Omega_t} a(\boldsymbol{U}(t,\boldsymbol{\xi}),\boldsymbol{\xi})\ \boldsymbol{\phi}(t,\boldsymbol{\xi})\ dt \right\rangle_{\Omega_{\boldsymbol{\xi}}}. \tag{15}$$

In this paper, use is made of the convention that operators are linear with respect to variables appearing after a semicolon sign.

Any component of $\boldsymbol{U}$ being a (second order) functional depending on time and on the random reaction rates, it can be expanded as an infinite series:

$$U(t,\boldsymbol{\xi}) = \sum_{k=0}^{\infty} U_k(t)\ \Psi_k(\boldsymbol{\xi}), \quad U_k(t) \in L_2(\Omega_t). \tag{16}$$

However, for practical computations, the series has to be truncated. We denote $U^h(t,\boldsymbol{\xi})$ the approximation of $U(t,\boldsymbol{\xi})$ on the semi-discrete approximation space $\mathcal{V}^h \equiv V_{\boldsymbol{\xi}} \times L_2(\Omega_t) \subset \mathcal{V}$:

$$U^h(t,\boldsymbol{\xi}) = \sum_{k=0}^{P_{\boldsymbol{\xi}}} U_k(t)\ \Psi_k(\boldsymbol{\xi}). \tag{17}$$

Equations for the stochastic modes $\boldsymbol{U}_k(t)$ of the solution are derived from the variational form given in Eq. (13), after plugging the rates and solution stochastic expansions. For instance, the equation for the

$0 \leq k \leq P_{\boldsymbol{\xi}}$-th stochastic mode of the concentration [OH] is

$$\begin{aligned}
\frac{d[\mathrm{OH}]_k(t)}{dt}\ \left\langle \Psi_k^2 \right\rangle_{\Omega_{\boldsymbol{\xi}}} &= \sum_{i,j=0}^{P_{\boldsymbol{\xi}}} \left(\Gamma_{r,1}\right)_i(t)\ [\mathrm{H_2O}]_j(t)\ \left\langle \Psi_i \Psi_j \Psi_k \right\rangle_{\Omega_{\boldsymbol{\xi}}} \\
&+ \sum_{i,j,o=0}^{P_{\boldsymbol{\xi}}} \left(\Gamma_{r,2}\right)_i(t)\ [\mathrm{H_2O}]_j(t)\ [\mathrm{H}]_o(t)\ \left\langle \Psi_i \Psi_j \Psi_k \Psi_o \right\rangle_{\Omega_{\boldsymbol{\xi}}} \\
&+ \sum_{i,j,o=0}^{P_{\boldsymbol{\xi}}} \left(\Gamma_{r,5}\right)_i(t)\ [\mathrm{H_2O}]_j(t)\ [\mathrm{HO_2}]_o(t)\ \left\langle \Psi_i \Psi_j \Psi_k \Psi_o \right\rangle_{\Omega_{\boldsymbol{\xi}}} \\
&+ \sum_{i,j,o=0}^{P_{\boldsymbol{\xi}}} \left(\Gamma_{r,8}\right)_i(t)\ [\mathrm{H_2O}]_j(t)\ [\mathrm{O_2}]_o(t)\ \left\langle \Psi_i \Psi_j \Psi_k \Psi_o \right\rangle_{\Omega_{\boldsymbol{\xi}}} \\
&- 2 \sum_{i,j=0}^{P_{\boldsymbol{\xi}}} \left(\Gamma_{f,7}\right)_i(t)\ [\mathrm{H_2O_2}]_j(t)\ \left\langle \Psi_i \Psi_j \Psi_k \right\rangle_{\Omega_{\boldsymbol{\xi}}}, \qquad (18)
\end{aligned}$$

with

$$\begin{aligned}
\left\langle \Psi_i \Psi_j \Psi_k \right\rangle_{\Omega_{\boldsymbol{\xi}}} &\equiv \int_{\Omega_{\boldsymbol{\xi}}} \Psi_i(\boldsymbol{\xi})\ \Psi_j(\boldsymbol{\xi})\ \Psi_k(\boldsymbol{\xi})\ p_{\boldsymbol{\xi}}(\boldsymbol{\xi})\ d\boldsymbol{\xi}, \\
\left\langle \Psi_i \Psi_j \Psi_k \Psi_o \right\rangle_{\Omega_{\boldsymbol{\xi}}} &\equiv \int_{\Omega_{\boldsymbol{\xi}}} \Psi_i(\boldsymbol{\xi})\ \Psi_j(\boldsymbol{\xi})\ \Psi_k(\boldsymbol{\xi})\ \Psi_o(\boldsymbol{\xi})\ p_{\boldsymbol{\xi}}(\boldsymbol{\xi})\ d\boldsymbol{\xi}. \qquad (19)
\end{aligned}$$

These tensors are sparse and independent of the solution: they are computed once for all in a preprocessing stage.

2.4. Time integration

As a result of the Galerkin projection, one is thus left with the time-integration of a set of $n_S \times (P_{\boldsymbol{\xi}} + 1)$ coupled non-linear ODEs describing the evolution of the stochastic modes of $\boldsymbol{U}^h(t, \boldsymbol{\xi})$. The time integration of the set of ODEs is achieved by relying on the `DVODE` library [3] which uses an adaptive integration time-step appropriate to steep ODEs. This algorithm is used with low a tolerance error criteria, such that the time-integration error can be safely assumed negligible compared to the stochastic discretization error caused by expanding the solution on the finite dimensional space $\mathcal{V}^h$. Clearly, the error in the approximation can then be theoretically controlled by increasing the stochastic expansion order q. However, for such non-linear stiff chemical system, it has been shown [18] that for large uncertainty levels, the time-integration of the truncated system of ODEs becomes more and more unstable as the expansion order increases. Therefore, performing accurate simulations using high order stochastic spaces as described above is not feasible. To circumvent this difficulty, a different strategy was proposed in [12], where a low order (typically less than 4) piecewise polynomial approximation is used at the stochastic level, thus allowing for accurate and stable simulations provided that an appropriate partition of the parameter space $\Omega_{\boldsymbol{\xi}}$ is constructed. In the next section, we describe an rigorous error analysis method which will be the basis of the adaptive strategies discussed latter in Section 4. Since, an essential property of these adaptive schemes is to rely on independent problems over non-overlapping sub-domains of $\Omega_{\boldsymbol{\xi}}$, the error analysis is presented in the case of a unique domain to ease the presentation.

3. Error analysis

3.1. A posteriori error estimation

The methodology for estimating the stochastic discretization error in the approximated solution is now presented. To measure the error in the discrete solution $U^h(t, \boldsymbol{\xi})$ with regard to the exact solution $U(t, \boldsymbol{\xi})$,

one needs to consider an appropriate metric $\mathcal{J}$. Let this metric $\mathcal{J}$ be a differentiable functional of the solution. We want to minimize the difference between the measure of the exact solution $\mathcal{J}(U)$ and that of the approximated solution $\mathcal{J}(U^h)$. To this end, we define two Lagrangian to be

$$\begin{aligned} \mathcal{L} &\equiv \mathcal{J}(\boldsymbol{U}) + A(\boldsymbol{U};\boldsymbol{Z}), \quad \forall\, \boldsymbol{Z} = (Z_1 \dots Z_{n_S})^T,\ Z_i \in \mathcal{V}, \\ \mathcal{L}^h &\equiv \mathcal{J}(\boldsymbol{U}^h) + A(\boldsymbol{U}^h;\boldsymbol{Z}^h), \quad \forall\, \boldsymbol{Z}^h = \left(Z_1^h \dots Z_{n_S}^h\right)^T,\ Z_i^h \in \mathcal{V}^h, \end{aligned} \tag{20}$$

where Z_i and Z_i^h are Lagrange multipliers and the form A was given in (15). Let us consider the minimization of the difference between the two Lagrangian. At the optimal point, the difference $\mathcal{L} - \mathcal{L}^h$ is stationary and has zero derivative in all its variables; for instance, considering $\mathcal{L}$ we have:

$$\frac{\partial \mathcal{L}}{\partial \boldsymbol{Z}} = A(\boldsymbol{U};\boldsymbol{\phi}) = 0, \qquad \forall\, \boldsymbol{\phi} = (\phi_1 \dots \phi_{n_S})^T,\ \phi_i \in \mathcal{V}, \tag{21}$$

$$\frac{\partial \mathcal{L}}{\partial \boldsymbol{U}} = \mathcal{J}'(\boldsymbol{U};\boldsymbol{\phi}') + A'(\boldsymbol{U};\boldsymbol{\phi}',\boldsymbol{Z}) = 0 \qquad \forall\, \boldsymbol{\phi}' = \left(\phi_1' \dots \phi_{n_S}'\right)^T,\ \phi_i' \in \mathcal{V}, \tag{22}$$

since $\mathcal{J}$ is a functional depending on $\boldsymbol{U}$. The derivatives are considered in the Gâteaux sense:

$$\begin{aligned} \mathcal{J}'(\boldsymbol{U};\boldsymbol{\phi}') &= \lim_{\varepsilon \to 0} \frac{\mathcal{J}(\boldsymbol{U} + \varepsilon\, \boldsymbol{\phi}') - \mathcal{J}(\boldsymbol{U})}{\varepsilon}, \\ A'(\boldsymbol{U};\boldsymbol{\phi}',\boldsymbol{Z}) &= \lim_{\varepsilon \to 0} \frac{A(\boldsymbol{U} + \varepsilon\, \boldsymbol{\phi}';\boldsymbol{Z}) - A(\boldsymbol{U};\boldsymbol{Z})}{\varepsilon}. \end{aligned} \tag{23}$$

The stationary condition of the Lagrangian expresses that the constraint must be enforced (Eq. 21) and gives an expression for the Lagrange multiplier, or adjoint solution, as the solution of the adjoint equation (Eq. 22). Similarly proceeding with the Lagrangian of the discrete problem, it finally yields:

$$\begin{aligned} \mathcal{L} - \mathcal{L}^h &= \mathcal{J}(\boldsymbol{U}) - \mathcal{J}(\boldsymbol{U}^h) + A(\boldsymbol{U};\boldsymbol{Z}) - A(\boldsymbol{U}^h;\boldsymbol{Z}^h), \\ &= \mathcal{J}(\boldsymbol{U}) - \mathcal{J}(\boldsymbol{U}^h). \end{aligned} \tag{24}$$

Minimizing the difference in the Lagrangian then reduces to minimizing the approximation error of the numerical solution in the functional $\mathcal{J}$ sense. As shown in [2] and [15], the approximation error can further be expressed as:

$$\mathcal{J}(\boldsymbol{U}) - \mathcal{J}(\boldsymbol{U}^h) \simeq A(\boldsymbol{U}^h;\boldsymbol{Z} - \boldsymbol{\phi}^h) + r, \tag{25}$$

with

$$r = \int_0^1 \left[A''(\boldsymbol{U}^h + s\, \mathcal{E}_{\boldsymbol{U}};\mathcal{E}_{\boldsymbol{U}}^2,\boldsymbol{Z}) - \mathcal{J}''(\boldsymbol{U}^h + s\, \mathcal{E}_{\boldsymbol{U}};\mathcal{E}_{\boldsymbol{U}}^2)\right]\, s\, ds, \tag{26}$$

the remainder term, and where $\mathcal{E}_{\boldsymbol{U}} \equiv \boldsymbol{U} - \boldsymbol{U}^h$. The remainder term is seen to be quadratic in $\mathcal{E}_{\boldsymbol{U}}$ and can be neglected compared to the leading term of Eq. (25), provided that $\mathcal{E}_{\boldsymbol{U}}$ is small enough, *i.e.* if the numerical solution $\boldsymbol{U}^h$ is a sufficiently close approximation of the exact solution $\boldsymbol{U}$. The interested reader may find more details about the *a posteriori* stochastic error analysis in [15].

3.2. Error estimate

Finally, the error analysis in Eq. (25) leads us to the classical estimation of the discretization error which is expressed as

$$\eta \equiv \left|\mathcal{J}(\boldsymbol{U}) - \mathcal{J}(\boldsymbol{U}^h)\right| \simeq \left|A(\boldsymbol{U}^h;\boldsymbol{Z} - \boldsymbol{Z}^h)\right|, \tag{27}$$

where the test function $\boldsymbol{\phi}^h$ as been classically substituted by $\boldsymbol{Z}^h$.

In the following, the accuracy of the numerical simulation will be evaluated in terms of a functional $\mathcal{J}$ chosen as the weighted sum of the L_2-norm of the n_S species concentrations over the solution domain $\Omega_{\boldsymbol{\xi}} \times \Omega_t$:

$$\mathcal{J} = \sum_{i=1}^{n_S} w_i \int_{\Omega_{\boldsymbol{\xi}}} \int_{\Omega_t} \left(U_i^h(t,\boldsymbol{\xi})\right)^2 \, p_{\boldsymbol{\xi}}(\boldsymbol{\xi}) \, dt \, d\boldsymbol{\xi}. \tag{28}$$

The weights w_i, $i = 1, \ldots, n_S$ are chosen so as to normalize the contribution of the different species to the functional $\mathcal{J}$. The weights selection will be discussed in greater details in the next section.

It seen from Eq. (27), that to have an approximation η of the error on the numerical solution $\boldsymbol{U}^h$, the exact solution $\boldsymbol{U}$ is not required. However, the exact adjoint solution $\boldsymbol{Z}$ is required. As is usually done in the *a posteriori* error analysis, this exact adjoint living in an infinite dimensional space is replaced by a high discretization order numerical solution of the adjoint problem, *i.e.* one considers $\widetilde{\boldsymbol{Z}}$ a surrogate of $\boldsymbol{Z}$:

$$\eta \quad \equiv \quad \left|\mathcal{J}(\boldsymbol{U}) - \mathcal{J}(\boldsymbol{U}^h)\right| \simeq \left|A(\boldsymbol{U}^h; \widetilde{\boldsymbol{Z}} - \boldsymbol{Z}^h)\right|. \tag{29}$$

In practice, approximating $\boldsymbol{Z}$ by $\widetilde{\boldsymbol{Z}}$ is not a problem as long as the actual error done on the surrogate adjoint variable is negligible compared to that on the numerical solution of the adjoint problem $\boldsymbol{Z}^h$. To determine $\widetilde{\boldsymbol{Z}}$, the dual code used to compute $\boldsymbol{Z}^h$ is employed with a higher polynomial order discretization, say twice as high as for $\boldsymbol{Z}^h$. The approximation space associated to $\widetilde{\boldsymbol{Z}}$ is then $\left(\mathcal{V}^{\widetilde{h}}\right)^{n_S}$.

4. Adaption strategies

4.1. Stochastic finite element mesh

The enrichment of the stochastic approximation, to improve the discrete solution accuracy, is achieved relying on a piecewise orthogonal polynomials representation in the stochastic domain. The approach corresponds to a finite element methodology, with the essential property that the solutions over different stochastic elements are fully independent. The stochastic finite element mesh consists in a partition of the stochastic domain $\Omega_{\boldsymbol{\xi}} = [-1,1]^{n_R}$ into a collection of N_b non-overlapping elements ${\Omega_{\boldsymbol{\xi}}}^m$:

$$\Omega_{\boldsymbol{\xi}} = \bigcup_{m=1}^{N_b} {\Omega_{\boldsymbol{\xi}}}^m, \quad \text{with } {\Omega_{\boldsymbol{\xi}}}^m \equiv [\xi_1^{m,-}; \xi_1^{m,+}[\times \ldots \times [\xi_{n_R}^{m,-}; \xi_{n_R}^{m,+}[\qquad \forall m = 1, \ldots, N_b, \tag{30}$$

where the superscripts $+$ and $-$ refer to the upper and lower bound respectively in the domain range. At a given time $t \in \Omega_t$, a generic component $U^h(t,\boldsymbol{\xi})$ of the solution has for expression:

$$U^h(t, \boldsymbol{\xi} \in {\Omega_{\boldsymbol{\xi}}}^m) = \sum_{k=0}^{P_{\boldsymbol{\xi}}} U_k^m(t) \, \Psi_k^m(\boldsymbol{\xi}), \tag{31}$$

where the superscript m on the solution coefficients is used to stress the local character of the expansion valid over the stochastic element m. Since $\boldsymbol{\xi}$ is uniformly distributed on $\Omega_{\boldsymbol{\xi}}$, the local measure over a stochastic element is also uniform. As a result, the polynomials $\Psi_k^m(\boldsymbol{\xi})$ are simply rescaled and shifted multi-dimensional Legendre polynomials. Their definition can be extended outside the support of the stochastic element by setting $\Psi_k^m(\boldsymbol{\xi} \notin \Omega_{\boldsymbol{\xi}}) = 0$. These polynomials are then orthogonal:

$$\left\langle \Psi_i^m \, \Psi_j^{m'} \right\rangle_{\Omega_{\boldsymbol{\xi}}} = \delta_{ij} \, \delta_{mm'} \left\langle (\Psi_i^m)^2 \right\rangle_{\Omega_{\boldsymbol{\xi}}}. \tag{32}$$

The formulation on each stochastic element is thus formally similar to the expansion in Eq. (17) above, namely

$$U^h(t,\boldsymbol{\xi}) = \sum_{m=1}^{N_b} \sum_{k=0}^{P_{\boldsymbol{\xi}}} U_k^m \Psi_k^m(\boldsymbol{\xi}), \tag{33}$$

but corresponds to an enriched stochastic approximation space:

$$\mathcal{V}_{\boldsymbol{\xi}}^h = \text{span}\left\{\{\Psi_k^m\},\ m = 1, \ldots, N_b,\ k = 0, \ldots, P_{\boldsymbol{\xi}}\right\}, \tag{34}$$

whose dimension is $(P_{\boldsymbol{\xi}} + 1)N_b$.

4.2. Local error

The error analysis presented in the previous section was derived for an arbitrary but orthogonal stochastic basis. As a result, the global error estimation η in Eq. (29) remains valid for the piecewise polynomial approximation on the stochastic mesh in Eq. (34). However, the global error estimation η can be bounded as follows:

$$\eta \leq \sum_{m=1}^{m} \eta^m, \quad \eta^m \equiv \left| A_{\Omega_{\boldsymbol{\xi}}{}^m}(\boldsymbol{U}^h; \widetilde{\boldsymbol{Z}} - \boldsymbol{Z}^h) \right|, \tag{35}$$

where the form $A_{\Omega_{\boldsymbol{\xi}}{}^m}$ is defined as

$$A_{\Omega_{\boldsymbol{\xi}}{}^m}(\boldsymbol{U}^h; \widetilde{\boldsymbol{Z}} - \boldsymbol{Z}^h) \equiv \int_{\Omega_t} \int_{\Omega_{\boldsymbol{\xi}}{}^m} a(\boldsymbol{U}^h, \boldsymbol{\xi}) \left(\widetilde{\boldsymbol{Z}} - \boldsymbol{Z}^h \right) p_{\boldsymbol{\xi}}(\boldsymbol{\xi}) d\boldsymbol{\xi} dt. \tag{36}$$

An important point to stress is that since $\boldsymbol{U}^h$, $\boldsymbol{Z}^h$ and $\widetilde{\boldsymbol{Z}}$ being all expanded on the same mesh of $\Omega_{\boldsymbol{\xi}}$, they can be computed in an element-wise fashion, thanks to the local character of the polynomials Ψ_k^m.

Equation (35) provides a local error estimation for the m-th stochastic element of the partition of $\Omega_{\boldsymbol{\xi}}$. However, this expression is not convenient in practice as one does not want to adapt the mesh globally over the entire time-domain Ω_t. It is more useful to adapt the mesh "on the fly", based on an error estimation performed element-wise and for a fraction of the whole time-span only. Such procedure not only allows for additional computational savings as the stochastic mesh can change with time, but it also avoids the need to restart the computations over from the initial conditions as we iterate to adapt the stochastic mesh. Instead we proceed sequentially, advancing the solution over successive time intervals $[t_l, t_{l+1}]$, with constant time span $\Delta t \equiv t_{l+1} - t_l$ for simplicity: starting from the solution at time t_l, we seek for the partition of $\Omega_{\boldsymbol{\xi}}$ that meets an accuracy criterion, to be discussed below, over the time-interval. When the adapted mesh is found we proceed with the following time-interval. To do so, we need an error estimation $\eta^{l,m}$ which is localized both in the stochastic domain and in the current time span. This error estimation is directly derived from Eq. (35), restricting the time integration to the current time-interval with index l:

$$\eta^{l,m} \equiv \left| \int_{t_l}^{t_{l+1}} \int_{\Omega_{\boldsymbol{\xi}}{}^m} a(\boldsymbol{U}^h, \boldsymbol{\xi}) \left(\widetilde{\boldsymbol{Z}} - \boldsymbol{Z}^h \right) p_{\boldsymbol{\xi}}(\boldsymbol{\xi}) d\boldsymbol{\xi} dt \right|. \tag{37}$$

To simplify the notations in the previous equation, we have not made explicit the dependence with the time-interval index l of the stochastic mesh of $\Omega_{\boldsymbol{\xi}}$.

An important aspect is that this strategy requires additional procedures to define a local initial condition, at the beginning of the considered time-interval (t_l) from the solution at the end of the previous one ($[t_{l-1}, t_l]$). Simple projection procedures are used to construct these local initial conditions (see [12] for details).

Finally, the functional $\mathcal{J}$ (see Eq. (28)) used for the error estimation involves weights w_i, which balance the contribution of the species. These weights are necessary because the specie contents vary by several orders of magnitude from each other, and in time too, as the reaction advances. Numerical experiments have shown that the weights could be appropriately selected as:

$$w_i^{l+1} = \begin{cases} 0 & \text{if } \displaystyle\int_{t_l}^{t_{l+1}} \langle U_{h,i} \rangle_{\Omega_{\boldsymbol{\xi}}}\, dt = 0, \\ \left[\displaystyle\int_{t_l}^{t_{l+1}} \left\langle \left(U_{h,i}^l(\boldsymbol{\xi}) \right)^2 \right\rangle_{\Omega_{\boldsymbol{\xi}}} dt \right]^{-1} & \text{otherwise.} \end{cases} \tag{38}$$

4.3. Adaptive strategies

4.3.1. Refinement

To reduce the global error η and make sure it remains below a prescribed threshold, we choose to reduce the error in each stochastic element independently, such that the local error estimation remains below a prescribed error tolerance $\epsilon_\eta \geq 0$:

$$\eta^{l,m} \leq \epsilon_\eta \, \Delta t \, \left|{\Omega_{\boldsymbol{\xi}}}^{l,m}\right| \;\; l = 0, 1, \ldots, \; \forall \, m = 1, \ldots, N_b(l), \tag{39}$$

where $\left|{\Omega_{\boldsymbol{\xi}}}^{l,m}\right|$ is the volume of the m-th stochastic element in the l-th time-interval. This inequality gives a rigorous criterion for activating the refinement: the stochastic *a posteriori* error analysis provides an estimation of the local discretization error over a stochastic element over the time-interval.

However, $\eta^{l,m}$ gives no further information about the *structure* of the error such as its dependence with the stochastic discretization order or the size of the stochastic element along each of its dimensions. We are thus left with a local error estimation, but no further indication allowing to derive a rigorous or optimal way of decreasing this error by activating the most appropriate refinement procedure. To achieve the error reduction, several strategies may be thought of:

- increase the temporal discretization level (t-refinement),
- increase the order of the discretization of the stochastic element (p-refinement),
- decrease the size of the stochastic element (h-refinement).

As discussed above, the temporal discretization of the problem relies on a stiff integrator with an adaptive time-stepping. Thanks to the high level of sophistication of the time-integration procedure, the error due to the time-integration is deemed negligible compared to the contribution of the stochastic discretization. One is thus left with two alternative strategies to refine the stochastic discretization if the local error has been estimated to be above the tolerance ϵ_η: p- or h-refinement. Since it is not clear which strategy is the best, and to avoid high order discretizations because of the scaling of the stochastic basis dimension with the order q (see Eq. (8)), we will hereafter only consider h-refinement, *i.e.* refinement of the stochastic element mesh.

A crucial point is that we have no information available from the error estimation to decide along which stochastic dimensions the h-refinement should be performed to efficiently reduce the error. Since the stochastic domain for the considered problem has $n_R = 8$ dimensions, a naive uniform (isotropic) h-refinement of a stochastic element along all the dimensions is simply not an option: every refinement of a stochastic element would leads to $2^8 = 256 - 1$ new elements so the problem would quickly become intractable. Then, one needs some directional information to adapt the discretization in a more efficient way. A rigorous anisotropic error estimation would be desirable at this point, but such an estimator only exists in a deterministic framework and for low discretization order [16], and is not available yet in the stochastic context. Therefore, ad-hoc alternatives based on directional analysis of the solution over the stochastic element are proposed below.

4.3.2. Coarsening

In addition to refinement, evolution problems may also benefit from a coarsening procedure of the stochastic mesh. While not unusual in deterministic simulations, this issue has not been addressed yet in the stochastic context and is nonetheless of crucial importance when dealing with stochastic problems where needs for an enriched discretization of the stochastic space evolve in time. The interest for coarsening procedures was clearly demonstrated in [17] for an ignition problem involving a single random parameter: the solution of the ignition problem is steep and requires a refinement over a small area of $\Omega_{\boldsymbol{\xi}}$, that travels as time progresses. An efficient adaptive strategy should then be able to refine the stochastic mesh in the steep areas and later coarsen when the reaction front has moved away in the stochastic domain. Clearly, needs for coarsening will be even more important for problems involving a larger number of random parameters.

A possible coarsening strategy is evaluated in the following. The strategy rely on the (local) *a posteriori* error estimation, $\eta^{l,m}$, to detect stochastic elements susceptible to be coarsened. Specifically, a stochastic element is considered as a candidate for coarsening whenever its error estimation $\eta^{l,m}$ falls below ϵ_η/γ, where $\gamma > 1$ is the ratio between the maximum and minimal acceptable error and acts as a tolerance ratio. The coarsening itself consists in merging two neighboring stochastic elements, both being admissible for coarsening. To maintain, the mesh structure consisting of hyper-rectangles in $\Omega_{\boldsymbol{\xi}}$, two stochastic elements can be merged only if they are conform along their common boundaries. This condition raises additional difficulties especially when dealing with high dimensional problems.

4.4. Directional indicators

We now discuss two directional error indicators to be used as criteria in the h-refinement and coarsening procedures.

4.4.1. Directional partial variance indicators

We propose a first anisotropic error indicator $\eta^{l,m}_{\sigma,j}$ for the stochastic element m and time-interval l associated to the random parameter j (and a given specie). This indicator is defined as the total sensitivity index [19, 9] restricted to the stochastic element and associated to parameter j. The total sensitivity indexes measure the variability of the specie concentration with regards to the different random parameters. An important point is that the orthogonal polynomial expansion of the solution explicitly provides these sensitivity indexes [4] such that their evaluation is immediate. Specifically, we define

$$\left(\eta^m_j\right)^2 \equiv \left(\sigma^m_j\right) / \left(\sigma^m\right)^2 \qquad j = 1, \ldots, n_R, \tag{40}$$

where the time index has been omitted for clarity. In Eq. (40), $\left(\sigma^m\right)^2$ is the local variance of the specie concentration over the SE m, while $\left(\sigma^m_j\right)^2$ is the partial variance associated to the random parameter j:

$$\left(\sigma^m\right)^2 \equiv \sum_{k=1}^{P_{\boldsymbol{\xi}}} \left(U^m_k\right)^2_k \left\langle \left(\Psi^m_k\right)^2 \right\rangle_{\Omega_{\boldsymbol{\xi}}}, \qquad \left(\sigma^m_j\right)^2 \equiv \sum_{k \,\in\, \mathcal{P}^m_j} \left(U^m_k\right)^2 \left\langle \left(\Psi^m_k\right)^2 \right\rangle, \tag{41}$$

where

$$\mathcal{P}^m_j = \left\{ 1 \leq k \leq P_{\boldsymbol{\xi}} \backslash \left\langle \left(\partial \Psi^m_k / \partial \xi_j\right)^2 \right\rangle_{\Omega_{\boldsymbol{\xi}}} \neq 0 \right\}. \tag{42}$$

These indicators allow to compare the respective contributions of different stochastic directions to the variance. In fact, it is assumed reasonable to consider that the direction with the highest sensitivity index yields the highest contribution to the discretization error. Consequently, the refinement of the stochastic element, if needed, will be performed along the direction j having the highest indicator η^m_j. Procedures based on the sensitivity indexes will hereafter be referred as Directional Partial-Variance (DPV) procedures.

4.4.2. Directional jump indicators

The second type of directional indicators are based on the discrete solution jump across the stochastic element boundaries. Since the stochastic elements are hyper-rectangle, jumps are measured with respect to interfaces having normals along a direction j. For a stochastic element m, one has:

$$\eta^m_j \equiv \frac{\overline{\Delta_j U^{m,+}} + \overline{\Delta_j U^{m,-}}}{\left| \langle U^m \rangle_{\Omega_{\boldsymbol{\xi}}} \right|}, \tag{43}$$

with $\langle U^m \rangle_{\Omega_{\boldsymbol{\xi}}}$ the expected concentration of the specie over the stochastic element m at time l, and

$$\begin{aligned} \left(\overline{\Delta_j U^{m,+}}\right)^2 &\equiv \frac{1}{\left|\Gamma^{l,m,+}_j\right|} \int_{\Gamma^{m,+}_j} \left(\Delta_j U^{m,+}(\boldsymbol{\xi})\right)^2 \, d\boldsymbol{\xi}, \\ \left(\overline{\Delta_j U^{m,-}}\right)^2 &\equiv \frac{1}{\left|\Gamma^{m,-}_j\right|} \int_{\Gamma^{m,-}_j} \left(\Delta_j U^{m,-}(\boldsymbol{\xi})\right)^2 \, d\boldsymbol{\xi}, \end{aligned} \tag{44}$$

where $\Gamma_j^{m,+}$ and $\Gamma_j^{m,-}$ are the upper and lower (n_R-1)-dimensional boundaries of element m with normals in direction $\pm j$. $\Delta_j U^{m,+}$ and $\Delta_j U^{m,-}$ are the differences (jump) of the trace of the solution on $\Gamma_j^{m,+}$ and $\Gamma_j^{m,-}$ respectively. If the interface is on the boundary of $\Omega_{\boldsymbol{\xi}}$, the corresponding jump is set to zero. Furthermore, the solution being polynomial in each element, the integrals can be computed exactly. In fact, the main difficulty is here to deal with non-conform stochastic meshes. As for the DPV indicators, the jump-based indicators are used to decide which direction should be refined first (the one with the highest indicator).

4.5. Summary of the adaptive algorithm

The global adaption algorithm thus proceeds along successive time intervals $[t_l, t_{l+1}]$. For each interval, a two stage procedure is set up. In the first stage, the solution is advanced from t_l to t_{l+1} while refining the stochastic mesh to meet the accuracy criterion over every stochastic elements. In the second stage, an attempt to coarsen the mesh is performed to yield the discrete solution at $t = t_{l+1}$, before considering the next time interval.

The algorithm for a time interval l is:

* **Integration / refinement stage**

FOR all stochastic elements

1. solve the primal and dual problems and get local solution $\boldsymbol{U}^h$ and $\boldsymbol{Z}^h$ on $\Omega_{\boldsymbol{\xi}}^{l,m}$,
2. solve for $\widetilde{\boldsymbol{Z}}$ the local dual problem on a higher polynomial approximation,
3. compute the local errors estimates $\eta^{l,m}$ from Eq. (37),
4. IF $\eta^{l,m} > \epsilon_\eta \Delta t \left|\Omega_{\boldsymbol{\xi}}{}^{l,m}\right|$ THEN SE needs refinement:
   a) for each direction j, compute the highest $\eta_j^{l,m}$ over the species from Eq. (40) or Eq. (43),
   b) split the SE along the direction j having the highest directional error indicator,
   c) update the stochastic mesh

   ELSE IF $\eta^{l,m} < \epsilon_\eta \, \Delta t \left|\Omega_{\boldsymbol{\xi}}{}^{l,m}\right| / \gamma$ THEN mark stochastic element for coarsening,

REPEAT UNTIL all stochastic elements satisfy the refinement criteria.

* Coarsening stage

FOR all stochastic elements marked for coarsening

1. compute the maximum over the species of the directional error indicator $\eta_j^{l,m}$ from Eq. (40) or Eq. (43),
2. let j be the dimension with lowest directional error indicator,
3. IF neighboring stochastic element in directions j is also marked for coarsening and the two are conforms THEN
   a) merge the two stochastic elements,
   b) project solution on the coarse element,
   b) update stochastic mesh

REPEAT UNTIL all stochastic elements have been checked.

Remark.
The resolution of the adjoint equations for $\boldsymbol{Z}^h$ and $\widetilde{\boldsymbol{Z}}$ over a stochastic element involves the knowledge of the primal solution $\boldsymbol{U}^h$ along the time-interval. As said above, the time-integrations use the `DVODE` solver which is based on automatic time-step adaptation, such that for the adjoint problem one has to provide values for $\boldsymbol{U}^h$ at intermediate times, not known a priori, in $[t_l, t_{l+1}]$. To circumvent this issue, a polynomial approximation of $\boldsymbol{U}^h(t)$ is used for the resolution of the adjoint problems. This polynomial approximation formally deteriorates the accuracy of the adjoint computation, but for the numerical parameters retained in the computations presented in the next section, in particular the span Δt of the time-intervals, the loss of accuracy was found negligible and not to affect the error estimation accuracy. In fact, a linear approximation between initial and final states $\boldsymbol{U}^h(t_l)$ and $\boldsymbol{U}^h(t_{l+1})$ can be safely used provided that Δt is not too large.

5. Results

We now present simulation results to demonstrate the efficiency of the proposed adaptive strategies. To ease the analysis, we consider in Section 5.1 a simplified version of the stochastic problem, where only two reaction rates are uncertain. This simplification allows us to perform extensive tests, to construct a reference solution and to study the impact of the different adaptation strategies without having to deal with a high dimensional issues. Then, in Section 5.2 we return to the original problem with 8 uncertain parameter and assess the algorithm performance for a high-dimensional problem.

5.1. Simplified stochastic problem

To start with, only reactions # 7 and 8 are considered uncertain, while rates for the other reactions are taken deterministic and equal to their respective median values (see Table 1). As a result, the stochastic domain has two dimensions only and the stochastic parameterization uses two random variables ξ_7 and ξ_8.

5.1.1. Reference solution

As a first step, a reference solution is computed with a first order polynomial discretization in the stochastic space ($q = 1$). The reference solution is constructed on a regular mesh involving a fixed grid of 180×180 stochastic finite elements of constant size. The first two statistical moments of the content in hydrogen [H] are plotted in Fig. 1 for this reference solution. These first moments denote the steep evolution of the stochastic solution in time after a short initiation stage. For $t > 1$, the evolution is much slower and for $t > 6$ the system experiences a slow evolution toward its asymptotic equilibrium state, which is independent of the uncertainty rates (ratii of forward to reverse rates are deterministic). It is noted that the variance, initially null (deterministic content), grows extremely fast and reaches a high level. In fact, the variance grows at a faster rate than the mean value during the initial stage. This large variance of the hydrogen content denotes the large sensitivity of the solution with regard to the reaction rates: small changes in Γ_7 and Γ_8 values induce large changes in the reaction dynamics. This feature pleads for the use of sophisticated techniques to accurately and efficiently represent the dependence of the solution with the rates.

5.1.2. Uniform refinement

We now apply the adaptive algorithm on the 2-D problem, starting from an regular mesh involving 2×2 stochastic elements at $t = 0$. A time span $\Delta t = 0.05$ is used for the adaptation, while no coarsening is allowed.

In a first series of simulation, we investigate the effect of the polynomial order q on the resulting stochastic mesh at $t = 10$ (s). Simulation are performed for $q = 0, 1$ and 2 and a constant error tolerance $\epsilon_\eta = 7.10^{-9}$ to trigger the refinement. In these simulations, the refinement is made uniform, *i.e.* a refined stochastic element is split into 4 equal sub-elements, to get rid of any effect due to the directional indicators. In addition, a minimal size is prescribed for the stochastic elements to limit the refinement. The stochastic meshes are shown in Fig. 2. It is observed that as the order of the discretization increases a coarser mesh is needed to satisfy the error tolerance on the solution.

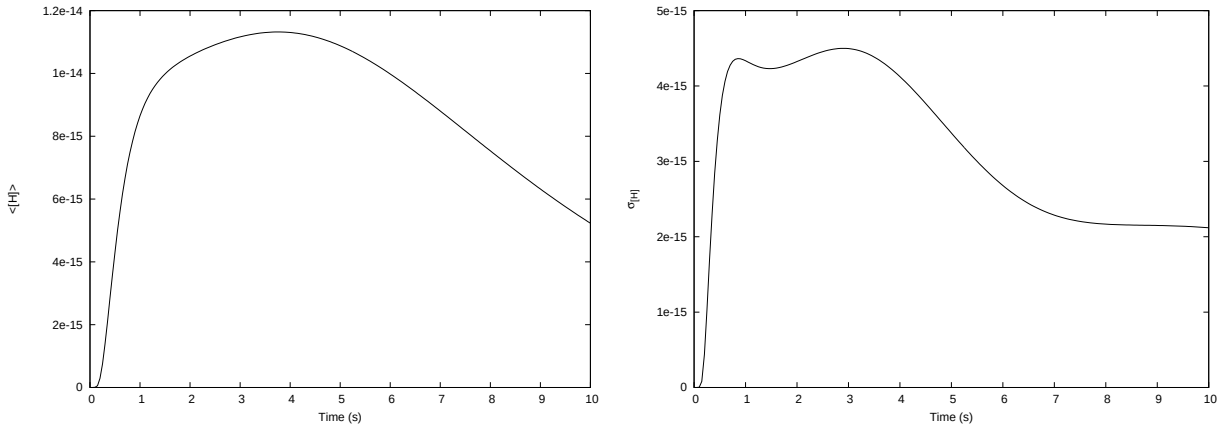

Figure 1: Mean (left) and standard deviation (right) of [H] as a function of time for the reference solution. Uncertainty in rates # 7 and 8 only.

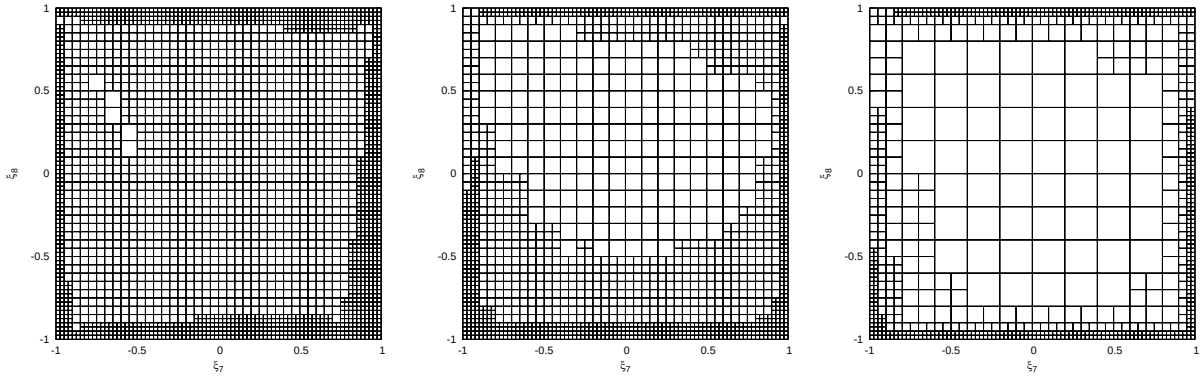

Figure 2: Stochastic finite element mesh of the 2-D stochastic domain at $t = 10$ s for different discretization orders q. From left to right: $q = 0$, 1, 2. $\epsilon_\eta = 7.10^{-9}$, uniform refinement, no coarsening.

The influence of the discretization order q onto the time-evolution of the number of stochastic elements as driven by the adaptation algorithm is plotted in Fig. 3. It is seen that the number of stochastic elements essentially varies at early times, as expected from the discussion of the reference solution. Latter, a slower refinement of the stochastic mesh is observed.

Further, it is seen from Fig. 2 that the refinement procedure leads to finer stochastic elements mainly concentrated at the boundary of the stochastic domain, while the central domain is not as much refined. Increasing q primarily leads to coarser elements also in the center part of the domain while fine elements are still needed along some part of the boundary. This behavior is due to the parameterization of the uncertain reaction rates and their log-normal distribution. Indeed as ξ_7 and ξ_8 goes to ± 1, the corresponding rates goes to 0 or $+\infty$. The mapping of the forward reaction rate $\Gamma_{f,7}$ as a function of ξ_7 is shown in the left plot Fig. 4 for illustration purpose (note that the reverse rate has an opposite trend). The variations of the rates with ξ_7 and ξ_8 directly translate to the solution steepness (with regard to the random parameters). This can be better appreciated from the surface response of the hydrogen content at the final time $t = 10$ s, shown in the right plot of Fig. 4. The steep dependence of [H] near the stochastic domain boundary is clearly exhibited. On the contrary, the solution is much smoother at the center of the domain, allowing for coarser stochastic elements when the order q is increased, while along the boundaries increasing the polynomial order is less efficient in reducing the error. This behavior demonstrates that the error estimation is able to

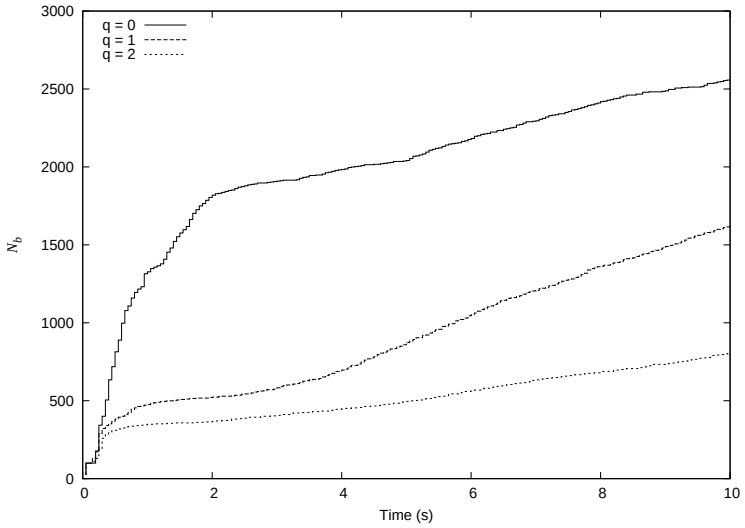

Figure 3: Number N_b of stochastic elements with time, for simulation order $q = 0, 1, 2$.

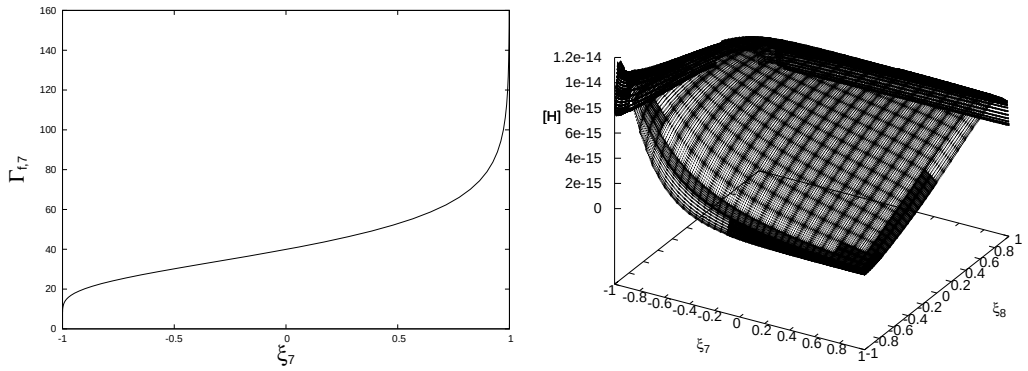

Figure 4: Left: parameterization of the log-normal forward rate $\Gamma_{f,7}$ as a function of ξ_7. Right: Response surface for the hydrogen content [H] at $t = 10$ s. Spectral discretization order $q = 1$, uniform refinement with $\epsilon_\eta = 4.10^{-9}$ and no coarsening.

properly determine which stochastic elements require refinement, and areas of the stochastic domain which are sufficiently discretized. In fact, these simulations indicate that a more effective strategy would consist in an adaptation where one decides for either h or p-refinement depending on the local smoothness of the solution.

5.1.3. Directional refinement

The impact of the selected refinement directional indicator, discussed in sections 4.4.1 and 4.4.2, is now investigated. The indicators being different, the adaptation processes result in different stochastic meshes, even if the error tolerance used is the same in the two cases. The meshes for the two-indicators however exhibit comparable number of elements for the two directional indicators and same ϵ_η, with differences in the meshes structure essentially limited to the immediate neighbor of the stochastic domain boundary. In fact, the treatment of the jump-based directional indicators for elements with interfaces on the boundary of $\Omega_{\boldsymbol{\xi}}$ are most probably the origin of the differences.

In Fig. 5, we compare the norms of the error (based on the reference solution, obtained for the two

directional indicators and the same tolerance ϵ_η. The error norms is defined as

$$\epsilon^2(t) = \left\langle \left([\mathrm{H}]^\star - [\mathrm{H}]^h \right)^2 (t) \right\rangle_{\Omega_{\boldsymbol{\xi}}} / \left\langle \left([\mathrm{H}]^\star \right)^2 (t) \right\rangle_{\Omega_{\boldsymbol{\xi}}}, \tag{45}$$

where $[\mathrm{H}]^\star$ is the discrete reference solution. Since for the two indicators the number of stochastic elements are close, we can deduce from Fig. 5 that the two indicators perform equally well in discriminating the stochastic dimensions requiring refinement. However, while performing as well as the DPV indicator, the jump-based approach is more computationally expensive, as it requires information from neighboring elements and to deal with non-conform meshes. On the contrary, the DPV indicator relies on elemental information solely, a property which makes the DPV approach more suitable for higher dimensional problem. Considering all these aspects, the DPV approach is retained throughout the remainder of the paper.

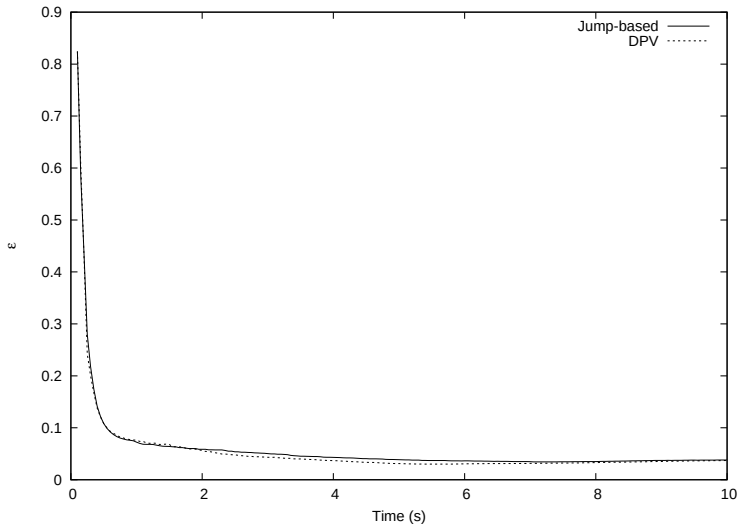

Figure 5: Error time-evolution for the anisotropic refinement based on the two directional indicator. $\epsilon_\eta = 7.10^{-9}$.

5.1.4. Error tolerance

To complete the series of 2-D simulations, we present in Fig. 6 the impact of the selected error tolerance criterion ϵ_η on the time evolution of the number of stochastic elements in the mesh and on error norm. Again, the h-refinement uses the DPV criteria, $q = 1$, and proceeds from an initial 2×2 stochastic mesh at $t = 0$. It is seen that as the tolerance is tightened the error clearly decreases at the price of a larger number of stochastic elements.

5.2. 8-D uncertain problem

We now consider the full uncertain chemical system with all rates uncertain, with properties listed in Table 1. The parameterization now involves n_R random variables so the stochastic domain has 8 dimensions. However, the uncertainty in the rates having different levels, and because of the complex dynamics of the chemical mechanisms, the dependence of the solution along the stochastic dimensions are very different [12]. Note that the uncertainty on the rates for reaction 7 and 8, which were considered in the previous simplified problem, are those with the largest and more complex impact on the solution.

This complex dependence of the solution with regard to the random parameters makes the problem very difficult and extremely demanding for the anisotropic refinement strategy to construct adapted stochastic meshes, with a tractable number of stochastic elements. We also recall that for simulations without piecewise polynomial decomposition, the Galerkin formulation is unstable, even for large order expansions.

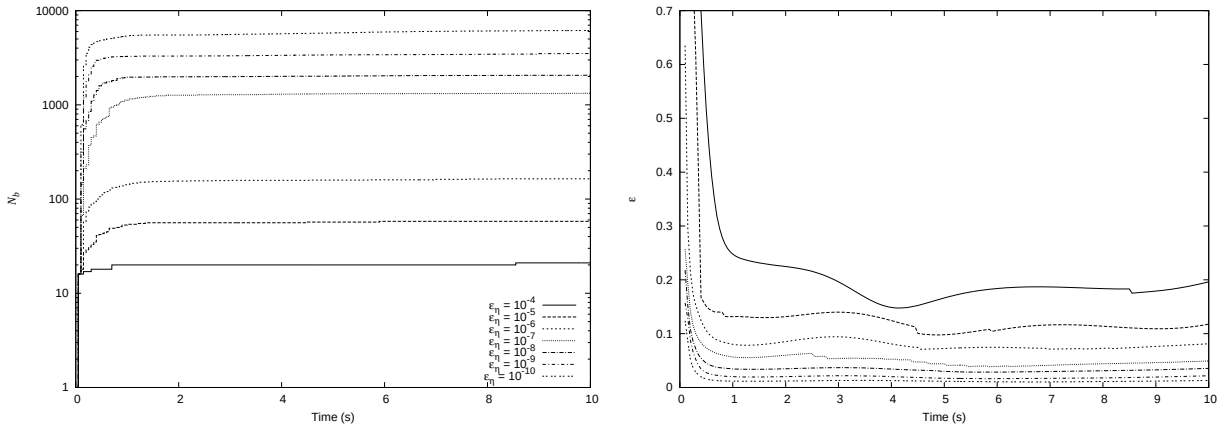

Figure 6: Time evolution of the number of blocks for different error tolerance ϵ_η (left). Corresponding solution error ϵ (right). From top to bottom, $\epsilon_\eta = 10^{-4}, 10^{-5}, 10^{-6}, 10^{-7}, 10^{-8}, 10^{-9}, 10^{-10}$.

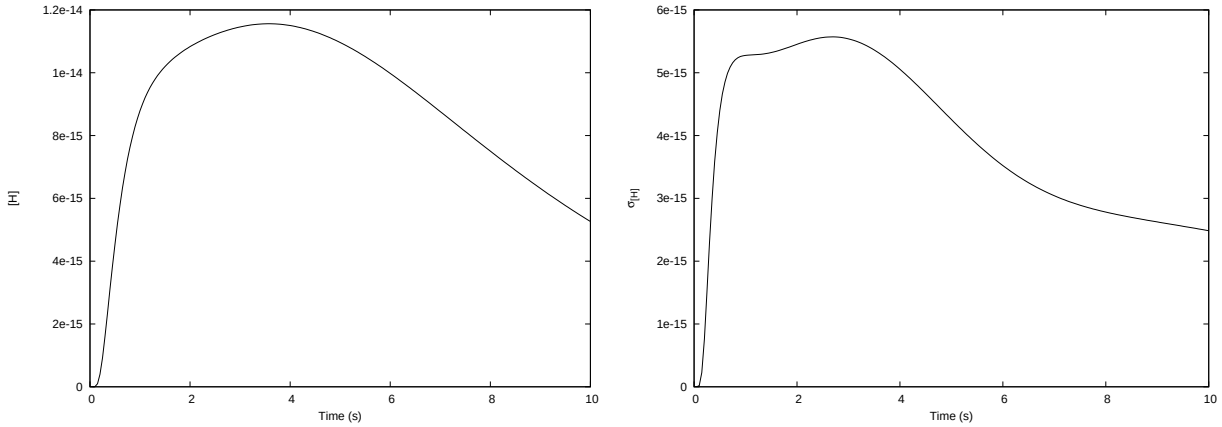

Figure 7: Time evolution of the mean (left) and variance (right) of the hydrogen content. 8-D stochastic problem.

We present below two simulations for the full problem. In the first one, only the refinement is performed, starting from a 2^{n_R} grid of stochastic elements with equal size. The anisotropic refinement uses the DPV indicator. Again, a limitation is set on the refinement to avoid stochastic elements with too low volume. The simulation uses $q = 1$ with an error tolerance $\epsilon_\eta = 1.75\ 10^{-8}$. The second simulation uses the same refinement procedure and numerical parameters, but we allow for coarsening with $\gamma = 4$ and, again, the DPV indicator.

In Fig. 7, we present the time evolution of the mean and standard deviation in [H], as computed with the refinement only. These results are in excellent agreement with the simulation presented in [12], which rely on multi-resolution scheme and multiwavelet expansions of the solution, with an isotropic adaptation criterion based on ideas similar to the DPV indicator (but without error estimation). The results for the simulation with coarsening are not shown as they are indistinguishable from the results with refinement only.

The effect of the refinement-only or refinement/coarsening strategy is shown in Fig. 8 where the number of required stochastic elements is plotted in time. As for the 2-D case, the error analysis triggers refinement at short times to capture the stiff behavior induced by the fast scale reactions. After some time, the number of blocks levels-off indicating that no further refinement is necessary. If coarsening is allowed, it is

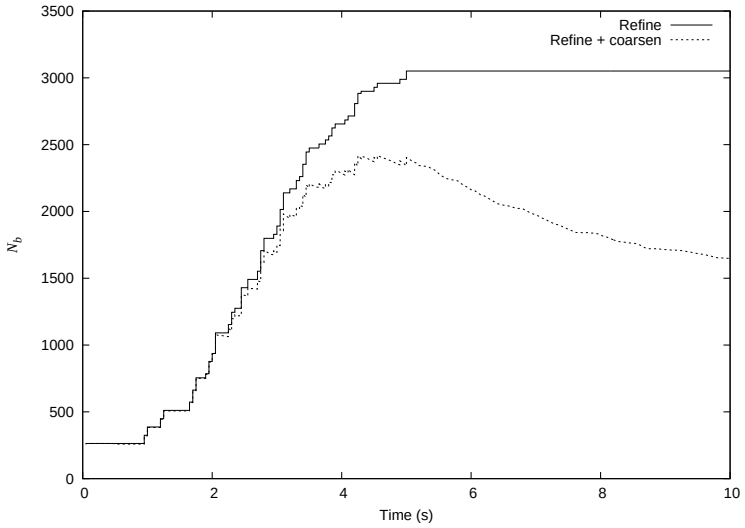

Figure 8: Time evolution of the number of blocks N_b for the refinement-only and the refinement-coarsening strategies. $q = 1$, $\epsilon_\eta = 1.75\ 10^{-8}$, $\gamma = 4$.

seen to strongly reduce the number of blocks while the solution error is kept within the same prescribed tolerance ϵ_η. At early times, the number of blocks is seen to be essentially the same as with the refinement-only procedure but, after some time, the fast reactions have occurred and a slower dynamics sets in with smoother dependences in the stochastic domain, hence calling for coarsening.

A somewhat finer picture of the mesh management strategy can be gained examining Fig. 9 where the distributions of the size of the blocks along dimension 4 and 7 are plotted. From Fig. 9 (right), they are seen to be refined along dimension 7 at early times while virtually no coarsening is observed for $0 < t < 10$ s. This denotes a stiff dependence to dimension 7, as already stated in the 2-D section. In contrast to this behavior, blocks along dimension 4, Fig. 9 (left), are seen to be also initially refined (the ratio of small blocks along dimension 4 increases) but, after some time ($t \gtrsim 4$), coarsening occurs and some larger blocks result from merging. Similar general behaviors may be observed from the other dimensions, not shown for sake of conciseness.

A global view of the blocks size time-evolution can be gained from Fig. 10 where the distribution of the volume of the blocks is plotted in time. The mesh is initialized with blocks of unit volume and is refined at short times, giving rise to small volume blocks. After $t \gtrsim 4$, coarsening occurs and some of the smallest blocks merge to result in bigger ones. The resulting mesh then involves a wide range of blocks size, allowing for an efficient adaptation of the solution approximation.

From the numerical point of view, the coarsening capability does not introduce a significant additional cost compared to the refinement-only strategy while leading to a strongly reduced number of blocks for the same accuracy. Indeed, coarsening criteria rely on the same quantities as those used for refinement (block local error estimation, directional contributions to the local variance). The additional cost essentially comes from the determination of the neighboring blocks and the check of conformity, if relevant. In this work, these steps were not CPU time consuming and no particular strategy was employed but it may become an issue if considering a higher dimensional problem involving tens or hundreds of dimensions. Efficient strategies may then be used for the mesh properties storage in memory. Further, alternative (*e.g.* hierarchical) mesh topology may be used to circumvent this potential issue and are the subject of on-going work.

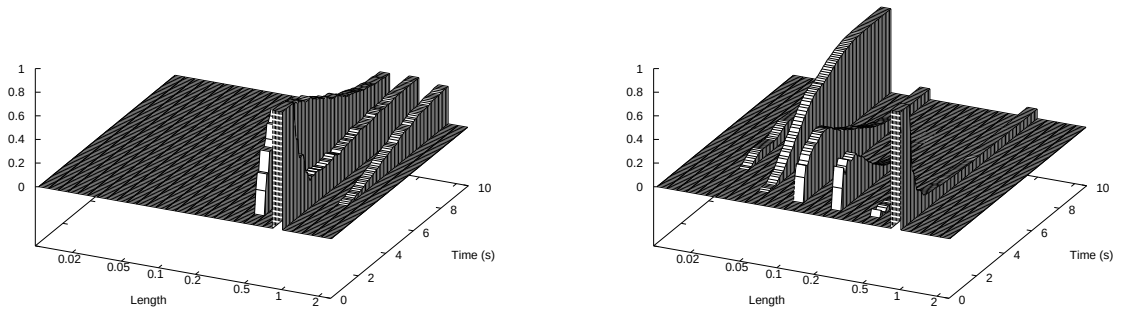

Figure 9: Time-evolution of the distribution of blocks size along dimension 4 (left) and 7 (right). $q = 1$, $\epsilon_\eta = 1.75\ 10^{-8}$, $\gamma = 4$.

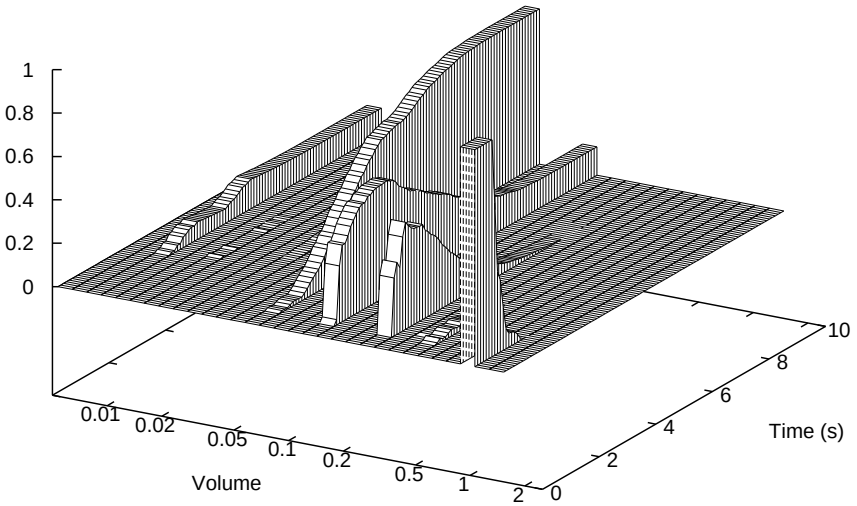

Figure 10: Time-evolution of the blocks volume distribution. $q = 1$, $\epsilon_\eta = 1.75\ 10^{-8}$, $\gamma = 4$.

6. Conclusion

This paper has discussed adaptation procedures for the stochastic discretization of the solution of uncertain chemical models. First, the dual-based *a posteriori* error analysis proposed in [15] was extended to the stochastic chemical model equations. The method relies on solving both a primal and two adjoint stochastic problems. At the expense of these additional dual computations, an accurate error estimation in each elements of the discretization space is available and adaptive strategies may be used to properly enrich the stochastic discretization and meet some accuracy criteria while maintaining a stochastic basis with reasonable dimension.

Based on this rigorous expression for the error estimation, different adaption strategies were proposed. In particular, an anisotropic strategy, for both stochastic refinement and coarsening, was discussed and tested in the results section on a hydrogen oxidation in supercritical conditions problem with uncertain reactions rates. This constitutes a high dimensional stiff uncertainty quantification problem which solution is difficult to get without a specific and efficient numerical technique. The present method was shown to perform well at a reasonable computational cost.

Several issues remain to be further investigated. A critical point of the a posteriori estimation is that it does not distinguish the directional components of the error. To circumvent the absence of rigorous anisotropic error estimators, we rely in this work on empirical anisotropic error indicators, based on directional contributions to the local variance or on jumps of the solution across stochastic sub-domains. Although this empirical indicators were shown to give satisfactory results, rigorous estimators would clearly improve the adaptation procedure and its reliability. This is the central focus of on-going works. Similarly, the coarsening procedure considered here could be greatly improved by relying on more appropriate data structures for the description of the stochastic discretization. The objective is here to construct (through refinement and coarsening) stochastic meshes with higher level of conformity between neighboring stochastic elements, in order to achieve higher acceptance rate at the coarsening stage of the present method.

References

[1] M. Abramowitz and I. Stegun. *Handbook of mathematical functions*. Dover, 1970.

[2] R. Becker and R. Rannacher. An optimal control approach to a posteriori error estimation in finite element methods. *Acta Numer.*, 10:1–102, 2001.

[3] P. Brown, G. Byrne, and A. Hindmarsh. VODE: a variable-coefficient ODE solver. *SIAM J. Sci. Statistical Computing*, 10(5):1038–1051, 1989.

[4] T. Crestaux, O. Le Maître, and J.-M. Martinez. Polynomial chaos expansion for sensitivity analysis. *Reliab. Eng. and Syst. Safety*, 2009. in press, doi:10.1016/j.ress.2008.10.008.

[5] M.K. Deb, I.M. Babuška, and J.T.Oden. Solution of stochastic partial differential equations using galerkin finite element techniques. *Comp. Methods Appl. Mech. Eng.*, 190(48):6359–6372, 2001.

[6] R.G. Ghanem. Probabilistic characterization of transport in heterogeneous media. *Trans. Porous Media*, 32:239–262, 1998.

[7] R.G. Ghanem and P.D. Spanos. *Stochastic finite elements. A spectral approach*. Dover Publications, Inc., rev. edition, 2003. 222 p.

[8] T.D. Hien and M. Kleiber. Stochastic finite element modeling in linear transient heat transfer. *Comp. Meth. App. Mech. Eng.*, 144:111–124, 1997.

[9] T. Homma and A. Saltelli. Importance measures in global sensitivity analysis of nonlinear models. *Reliab. Eng. and Syst. Saf.*, 52(1):1–17, 1996.

[10] M. Kaminski and T.D. Hien. Stochastic finite element modeling of transient heat transfer in layered composites. *Int. Com. Heat and Mass Trans.*, 26:801–810, 1999.

[11] O.P. Le Maître, H.N. Najm, R.G. Ghanem, and O.M. Knio. Multi-resolution analysis of Wiener-type uncertainty propagation schemes. *J. Comp. Phys.*, 197(2):502–531, 2004.

[12] O.P. Le Maître, H.N. Najm, P.P. Pébay, R.G. Ghanem, and O. Knio. Multi-resolution analysis for uncertainty quantification in chemical systems. *SIAM J. Sci. Comp.*, 29(1):864–889, 2007.

[13] O.P. Le Maître, M.T. Reagan, B. Debusschere, H.N. Najm, R.G. Ghanem, and O. Knio. Natural convection in a closed cavity under stochastic, non-boussinesq conditions. *SIAM J. Sci. Comp.*, 26:375–394, 2004.

[14] O.P. Le Maître, M.T. Reagan, O.M. Knio, H.N. Najm, and R.G. Ghanem. A stochastic projection method for fluid flow. ii. random process. *J. Comp. Phys.*, 181(1):9–44, 2002.

[15] L. Mathelin and O.P. Le Maître. Dual-based a posteriori error estimate for stochastic finite element methods. *Comm. App. Math. Comp. Sci.*, 2:83–115, 2007.

[16] S. Micheletti, S. Perotto, and M. Picasso. Stabilized finite elements on anisotropic meshes: a priori error estimates for the advection-diffusion and the stokes problems. *SIAM J. Numer. Anal.*, 41(3):1131–1162, 2003.
[17] H.N. Najm, B.J. Debusschere, Y.M. Marzouk, S. Widmer, and O.P. Le Maître. Uncertainty quantification in chemical systems. *Int. J. Numer. Meth. Engng*, pages 499–522, 2009. in press DOI: 10.1002/nme.2551.
[18] M. Reagan, O. Le Maître H. Najm, B. Debusschere, O.M. Knio, and R.G. Ghanem. Spectral stochastic uncertainty quantification in chemical systems. *Combustion Theory and Modelling*, 8:607–632, 2004.
[19] I.M. Sobol. Sensitivity estimates for nonlinear mathematical models. *Math. Mod. and Comput. Exp.*, 1(4):407–414, 1993.
[20] C. Soize and R. Ghanem. Physical systems with random uncertainties : chaos representations with arbitrary probability measure. *J. Sci. Comput.*, 26(2):395–410, 2004.
[21] X. Wan and G.E. Karniadakis. An adaptive multi-element generalized polynomial chaos method for stochastic diffential equations. *J. Comp. Phys.*, 209:617–642, 2005.
[22] N. Wiener. The homogeneous chaos. *Amer. J. Math.*, 60(4):897–936, 1938.
[23] D. Xiu and G.E. Karniadakis. Modeling uncertainty in flow simulations via generalized polynomial chaos. *J. Comp. Phys.*, 187:137–167, 2003.